*Sensors and Materials*, Vol. 34, No. 2 (2022) 745–756
MYU Tokyo



S & M 2849

# Radio-photoluminescence Properties of Heavy-element-based Alkaline Phosphate Glasses and Their Application to X-ray Imaging

Daiki Shiratori,* Yuma Takebuchi, Takumi Kato,
Daisuke Nakauchi, Noriaki Kawaguchi, and Takayuki Yanagida

Graduate School of Science and Technology, Nara Institute of Science and Technology,
8916-5 Takayama-cho, Ikoma, Nara 630-0192, Japan

(Received October 15, 2021; accepted November 25, 2021)

***Keywords:*** radio-photoluminescence, dosimeter, X-ray image, glass, photoluminescence

A glass phosphor is an attractive material for applications in radiation detection because of its high workability and availability with a wide range of chemical compositions. Recently, the X-ray-induced luminescence of glasses containing various luminescent activators has been actively investigated worldwide. Among them, glass that exhibits the radio-photoluminescence (RPL) phenomenon is a promising material for not only dosimetry but also X-ray imaging applications. However, there are only a few materials that exhibit the RPL phenomenon, and thus there is room for material exploration. In this study, we found that $Ag_2O$–$R_2O$–BaO–$Al_2O_3$–$P_2O_5$ ($R$ = K, Rb, Cs) glass, in which some of the constituents of the commercial RPL glass were replaced with heavy elements, shows RPL properties worthy of practical application. Our glass specimens have a spatial resolution of at least 8 LP/mm; furthermore, the fading of the emission from RPL centers was much lesser than that from commercial imaging plates.

## 1. Introduction

Phosphors have a very wide scope of applications in not only lighting, displays, and sensors that use stress luminescence but also radiation detection applications such as nuclear medicine,[1–4] environmental dose monitoring,[5] personal dose monitoring,[6–8] high-energy astronomy,[9–11] security,[12,13] and oil logging.[14–16] In these applications, radiation is measured by utilizing the monotonic change in the emission intensity of a phosphor with the energy of the irradiated ionizing radiation. Passive detectors, such as personal dosimeters, accumulate radiation energy once as carriers and read it out later as photoluminescence (PL). There are two types of dosimeter classified by different ways (energies) to stimulate carriers; the thermally stimulated luminescence (TSL) dosimeter uses thermal stimulation[17–21] and the optically stimulated luminescence (OSL) dosimeter utilizes light stimulation.[22–25] In contrast, some dosimeters use a phenomenon called radio-photoluminescence (RPL), in which luminescent centers corresponding to irradiation doses are newly generated, and RPL can be easily read out

*Corresponding author: e-mail: shiratori.daiki.sc3@ms.naist.jp
https://doi.org/10.18494/SAM3695

ISSN 0914-4935 
https://myukk.org/

by a PL technique. The most prominent RPL material is Ag-doped phosphate glass (RPL glass).[26,27] When RPL glass is irradiated by ionizing radiation, electron–hole pairs are generated, and $Ag^+$ ions are changed to $Ag^0$ by capturing electrons ($Ag^+ + e^- \rightarrow Ag^0$). On the other hand, some of the generated holes are once trapped in the $PO_4^{3-}$ tetrahedral, and moving along the $PO_4^{3-}$ network, the holes finally shift to $Ag^+$ with thermal treatments that are called build-up processes and form a more stable $Ag^{2+}$ ($Ag^+ + h^+ \rightarrow Ag^{2+}$). Both $Ag^0$ and $Ag^{2+}$ thus formed serve as the RPL centers in glass. One of the characteristics of RPL glass is that the luminescent center, once generated, does not fade. This property is useful for not only dosimetry applications but also X-ray imaging. In the case of X-ray imaging using an RPL material, there is no risk of blurring of the image due to the excitation light inducing emission other than the readout area, and thus a resolution higher than that with an OSL material can be expected. However, the RPL glass composed of light elements has a low probability of interaction with X-rays and requires a longer irradiation time for imaging; thus, the situation requires the development of an RPL material composed of heavy elements for the practical use of RPL imaging. In this study, we investigated the luminescence properties of FD-7, a commercial RPL glass (Na: 11.0 wt.%, P: 31.6 wt.%, O: 51.2 wt.%, Al: 6.1 wt.%, and Ag: 0.17 wt.%),[28] by replacing alkali metal species with another and adding Ba to the composition. Ba was selected with the intention of increasing the effective atomic number ($Z_{eff}$) of the glass. In addition, Ba can also be expected to improve the water resistance of the glass. The alkali metals in the glass combine with the oxygen in the structure to form non-bridging oxygen. They also readily react with water and elute, resulting in low water resistance and fading. Among them, Rb and Cs are particularly reactive owing to their weak bonding;[29] thus, it is expected that the reactivity with water and the hygroscopicity of glasses will also increase. On the other hand, Ba is present in the middle of the network structure of phosphate and is effective in improving the water resistance of glass by strengthening the bonds.[30–32] Furthermore, Ba is effective in increasing the density of glass.[33]

## 2. Materials and Methods

### 2.1 Specimen preparation

$Ag_2O$–$R_2O$–BaO–$Al_2O_3$–$P_2O_5$ ($R$ = K, Rb, Cs) glasses were prepared by the conventional melt-quenching method using an electric furnace. The starting materials of $K_2CO_3$ (4N), $Rb_2CO_3$ (3N), $Cs_2CO_3$ (4N), $BaCO_3$ (4N), and $Al(PO_3)_3$ (4N) were uniformly mixed at the molar ratio of 20:50:30 to $R_2CO_3$, $BaCO_3$, and $Al(PO_3)_3$, respectively. Thus, the obtained chemical composition of glass was $6.25R_2O$–$18.75BaO$–$18.75Al_2O_3$–$56.25P_2O_5$ (mol.%). We added $Ag_2O$ (4N) to the host glass so that the Ag content would be 1.00 mol.% relative to the host glass compositions ($0.50Ag_2O$–$6.25R_2O$–$18.75BaO$–$18.75Al_2O_3$–$56.25P_2O_5$). These powders were weighed in a total amount of 10.0 g and mixed homogeneously using an agate mortar. The mixed powder was put into an alumina crucible and then melted at 1300 °C for 30 min in air atmosphere. After the melting, the alumina crucible was quickly taken out from the furnace using a tongue to quench the glass melt on a stainless-steel plate preheated to 300 °C. Following the annealing

procedure, the glass specimens were cut into dimensions of 10.0 × 10.0 × ~1.0 $mm^3$ and then the surfaces were mechanically polished. In this study, each glass specimen containing K, Rb, and Cs will be described as Ag–K, Ag–Rb, and Ag–Cs, respectively.

### 2.2 Measurement method

The densities of the glass specimens were determined by the Archimedes method using analytical balances (GR-120, A&D Co., Ltd.). The glass transition temperatures ($T_g$) of the glass specimens were determined using a TG-DTA system (STA7200, Hitachi High-Tech Corporation) operating at a heating rate of 10 °C/min. X-ray diffraction (XRD) patterns were measured with MiniFlex 600 (RIGAKU) in order to verify the precipitation in the glass specimens.

Transmission spectra of the glass specimens were determined using a spectrophotometer (V670, JASCO) across a spectral range from 190 to 2700 nm with 1 nm intervals. To investigate the number of RPL centers produced by X-rays, the absorbance of UV light at 340 nm for the glass specimens was also measured using the spectrophotometer.

PL and RPL spectra were obtained using our lab-constructed setup. A xenon lamp (LAX-C100, Asahi Spectra) and an optical band-pass filter (RR0340, Asahi Spectra) were used to obtain a 340 ± 20 nm excitation light. The PL and RPL emission spectra were obtained with an optical short-cut filter (LU0400, Asahi Spectra) and a fiber-coupled lens, which guided the light to a CCD-based spectrometer (QEPro, Ocean Optics). The RPL spectrum was obtained by measuring the emission of the specimen after X-ray irradiation using an X-ray generator (XRBOP&N200X4550, Spellman). The resolution of the X-ray image was determined using the same optical system as that used in the PL measurement and a commercially available test chart (CN56284, Moriyama X-Ray Equipments Co., Ltd.). A glass specimen was irradiated with X-rays through a test chart, and then the specimen was excited with 340 nm UV light while the emission was read by a CCD camera (BU-54UV, Bitran) to obtain X-ray images. To determine the origin of luminescence, PL lifetime measurements were performed using Quantaurus-Tau (C11367, Hamamatsu Photonics).

## 3. Results and Discussion

The density, $T_g$, and $Z_{eff}$ of all the glass specimens and FD-7 are shown in Table 1. Among the glass specimens, the density of FD-7 was the lowest, and the glass with the heavy alkali metals has a higher density. Similarly, the Ag–Cs specimen has the highest $Z_{eff}$, and furthermore, the $Z_{eff}$ values of the glass specimens prepared in this study are much higher than that of FD-7. On

Table 1
Density, $T_g$, and $Z_{eff}$ of all glass specimens and FD-7.

| Specimen code | Density (g/$cm^3$) | $T_g$ (°C) | $Z_{eff}$ |
|---|---|---|---|
| FD-7 | 2.61 | 450 | 16.5 |
| Ag–K | 3.27 | 546 | 47.3 |
| Ag–Rb | 3.54 | 530 | 49.2 |
| Ag–Cs | 3.65 | 477 | 51.8 |

the other hand, the $T_g$ of each specimen tends to decrease as the alkali metal species in the composition become heavier elements. The XRD patterns of all the glass specimens are shown in Fig. 1. The glass specimens showed only a halo structure, which suggests that no crystallization had occurred during quenching. In other words, we have obtained glassy specimens.

Figures 2(a) and 2(b) show the linear transmission spectra of each glass specimen in the UV–VIS and UV–NIR regions, respectively. There is almost no difference in the spectra due to the difference in alkali metal species, and the absorption wavelengths of the glass specimens are almost the same. Compared with that of FD-7, the optical absorption edges of our glass specimens significantly shifted to the longer wavelength side. Furthermore, our specimens did not show the absorption due to hydroxy groups in the NIR region observed in FD-7, which indicates that Ba in the glass improved the water resistance. The difference in the transmittance

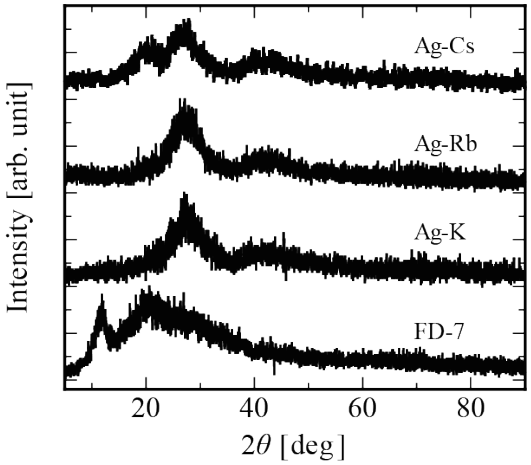


Fig. 1. XRD patterns of all glass specimens and FD-7.

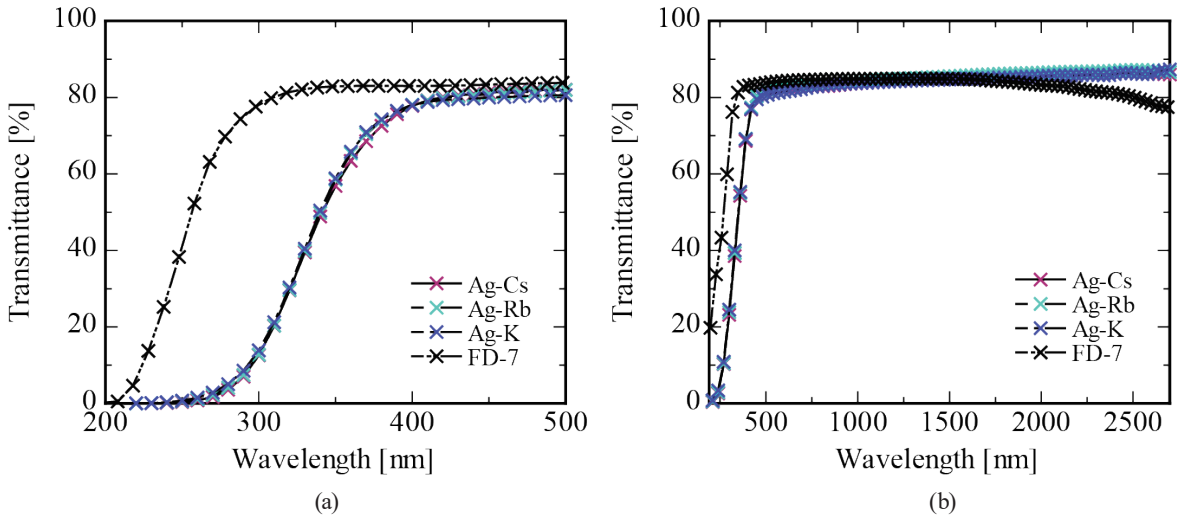


Fig. 2. (Color online) (a) UV–VIS and (b) UV–NIR region transmission spectra of the glass specimens and FD-7.

of each glass specimen is considered to be caused by the surface condition and thickness error of the glass specimen.

Figure 3 shows the PL spectra of all the glass specimens measured before and after X-ray irradiation (10 Gy). The excitation wavelength of each emission was 340 ± 20 nm. The pink dashed line in each figure shows the excitation spectrum after 10 Gy of X-ray irradiation. The PL spectra of each glass specimen showed differences before and after X-ray irradiation, but no significant change in the spectral shape due to the difference in the type of alkali metal was observed. All the glass specimens before X-ray irradiation showed emission peaking at around 440 and 530 nm. On the other hand, a broad emission at around 600 nm was newly observed in the spectrum after X-ray irradiation. The emissions at around 400 and 600 nm are assigned to $Ag^0$ or $Ag_2^+$ (monovalent Ag dimer) and $Ag^{2+}$ on the basis of previous reports on FD-7

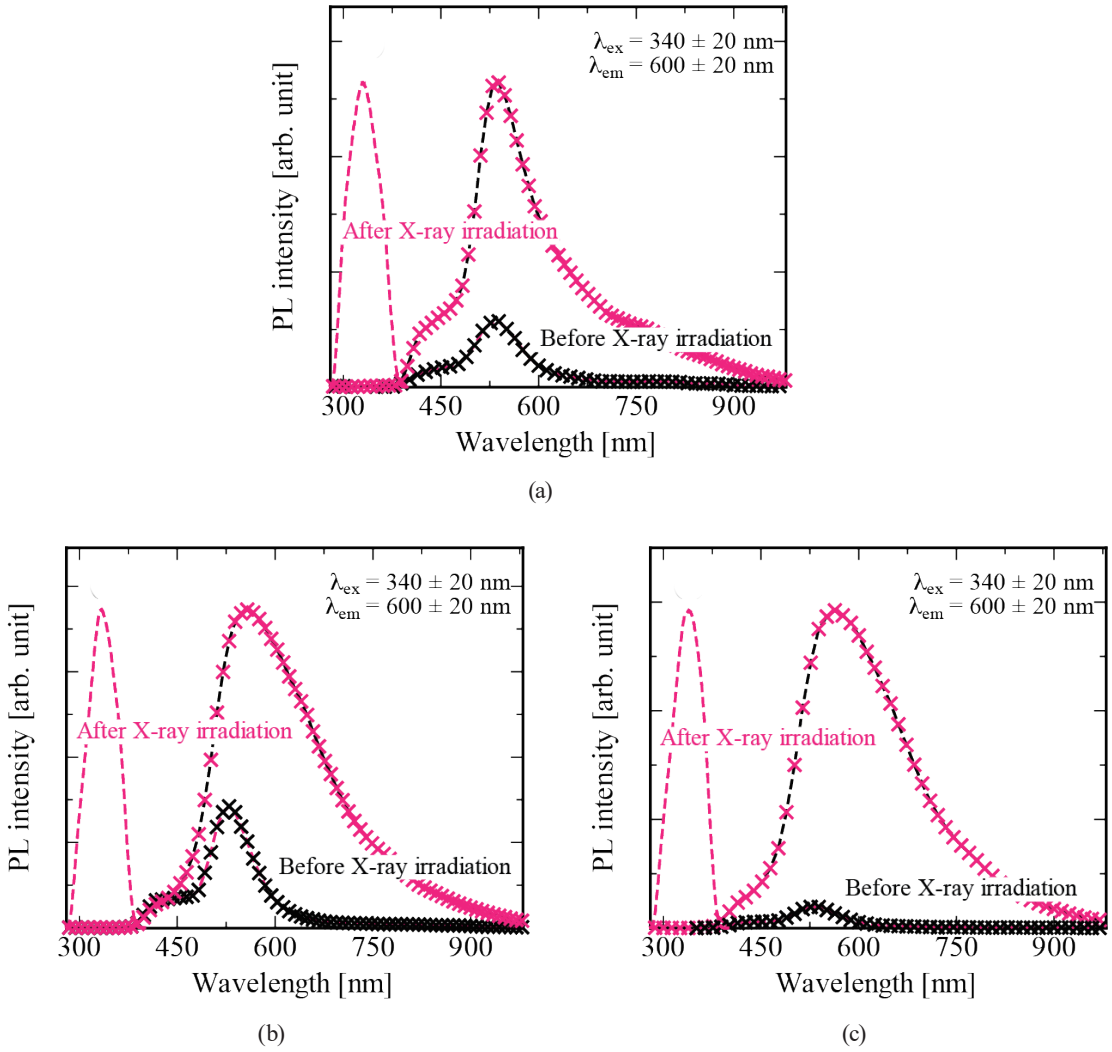


Fig. 3. (Color online) PL excitation and emission spectra of (a) Ag–K, (b) Ag–Rb, and (c) Ag–Cs specimens measured before and after X-ray irradiation (10 Gy). The excitation wavelength was 340 ± 20 nm.

luminescence, respectively.[34–37] On the other hand, the emission at around 530 nm is reasonable as the luminescence originating from the host glass, since the undoped specimen shows a similar emission band. These results demonstrate that $R_2O$–BaO–$Al_2O_3$–$P_2O_5$ glass exhibits RPL, and that the RPL phenomenon is not inhibited by alkali metal species.

Figure 4 shows the PL decay curves of the emission at around 650 nm when each specimen was excited by 340 ± 20 nm light. The decay curves can be approximated by a two-component exponential function, and the decay constants calculated from these curves are around 1.5 and 0.9 μs. These decay constants are generally consistent with the results of the lifetimes of FD-7 and Ag-doped $Li_2O$–$Al_2O_3$–$P_2O_5$ glass, as reported previously;[26,27,38] thus, the emission at around 650 nm is attributed to $Ag^{2+}$.

Table 2 shows the difference in the absorbance $\Delta A_{abs}$ of light at 340 nm for all the glass specimens before and after X-ray irradiation, and the value of $Z_{eff}$ to the fourth power. This variation in absorption at 340 nm represents the number of RPL centers ($Ag^{2+}$) formed. The formation of $Ag^{2+}$ was highest for the Ag–Cs glass specimen, and the values for the other specimens were very much the same. Here, $\Delta A_{abs}$ is presumed to depend on the absorption efficiency of X-rays ($Z_{eff}^4$) and the efficiency of $Ag^{2+}$ formation. As for the efficiency of $Ag^{2+}$ formation, it is reported that the larger the ionic radius of the alkali metal species in phosphate glass, the more the average molar volume increases and the more the distance between the $PO_4^{3-}$ tetrahedron and $Ag^+$ increases, which decreases the activation energy of $Ag^{2+}$ formation.[39]

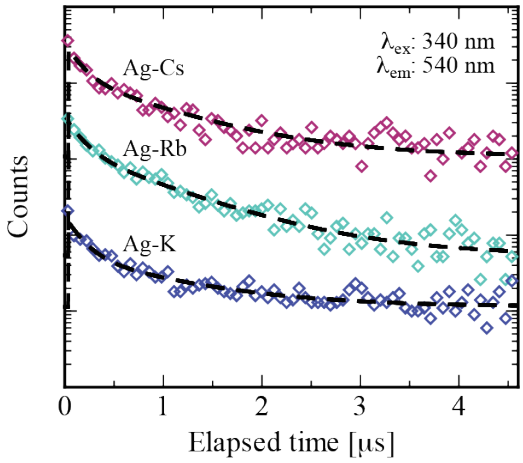


Fig. 4. (Color online) PL decay curves of all glass specimens and FD-7. The excitation and emission wavelengths of the glass specimens were 340 and 540 nm, respectively.

Table 2
Change in absorbance at 340 nm and $Z_{eff}^4$ of FD-7 and each glass specimen before and after 1 Gy of X-ray irradiation.

| Specimen code | $\Delta A_{abs}$ (arb. unit) | $Z_{eff}^4$ ($\times 10^5$) |
|---|---|---|
| FD-7 | 0.015 | 2 |
| Ag–K | 0.009 | 50 |
| Ag–Rb | 0.012 | 58 |
| Ag–Cs | 0.041 | 72 |

Therefore, it is expected that the efficiency of $Ag^{2+}$ formation will increase in the order of K < Rb < Cs. Therefore, it is reasonable to conclude that the Ag–Cs specimen with the highest $Z_{eff}^4$ and largest ionic radius has the highest number of RPL centers. On the other hand, the $\Delta A_{abs}$ values of the Ag–Rb and Ag–K specimens are lower than that of FD-7, which will be discussed in detail in the section on TSL glow curves.

Figure 5 shows a comparison of the RPL intensities of the specimens irradiated with 1 and 10 Gy of X-rays. Here, the RPL intensity is defined as the difference between the PL spectrum of the specimen irradiated with X-rays and the PL spectrum of the glass specimen before X-ray irradiation as background. In the specimens after 1 Gy of X-ray irradiation, Ag–Cs showed the highest RPL intensity, which was approximately twice the peak intensity of FD-7. The RPL intensity of each glass specimen showed a similar trend to the $\Delta A_{abs}$ results. On the other hand, when the specimen was irradiated with 10 Gy of X-rays, the RPL intensity of FD-7 increased significantly compared with those of the other glass counterparts. This result suggests that FD-7 has a more stable RPL center than our glass specimens (detailed in the section of TSL glow curves). In addition, we calculated the full widths at half maximum (FWHMs) of the RPL spectra after 10 Gy of X-ray irradiation, which were about 0.38, 0.61, 0.60, and 0.53 eV for Ag–K, Ag–Rb, Ag–Cs, and FD-7, respectively.

Figure 6 shows the build-up curves of RPL emissions for each glass specimen and FD-7. The vertical axis corresponds to the integrated intensity of the 400–900 emissions. The RPL intensity of the Ag–K specimen saturated immediately after irradiation, whereas those of the Ag–Rb and Ag–Cs specimens clearly showed the build-up phenomenon. Furthermore, all the glass specimens reached a steady state within 60 s. The time to saturation of the build-up of this glass specimen is particularly short among the Ag-doped RPL glasses reported to date. For example, the RPL intensity of FD-7 stabilizes after 1–2 h,[36] and in the case of $Na_2O$–$Al_2O_3$–$P_2O_5$–$SiO_2$ glass, it continues to increase for more than 12 h.[40] When RPL materials are used for radiation measurements, this build-up phenomenon becomes a hindrance during analysis. In

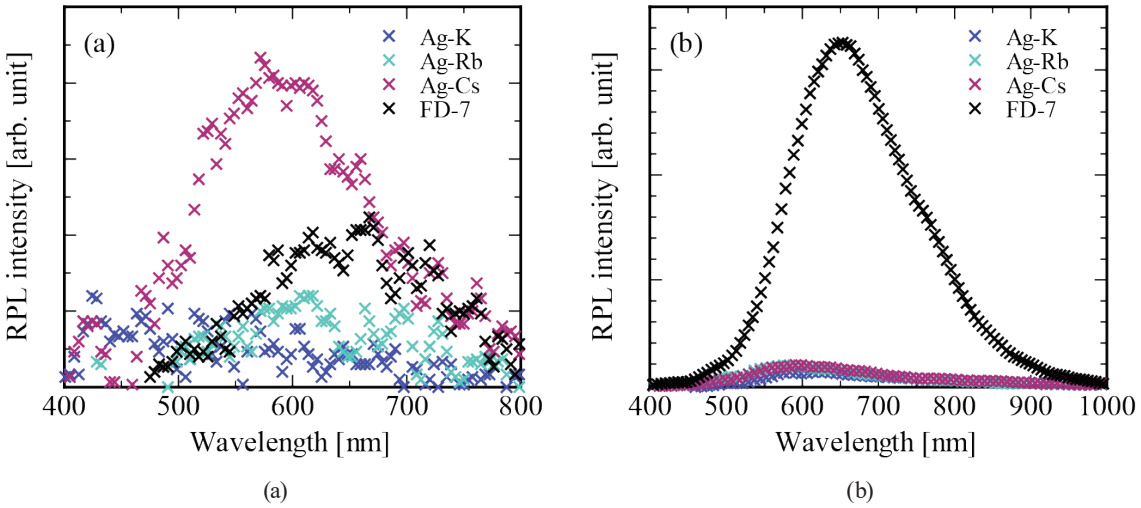


Fig. 5. (Color online) Comparison of RPL intensities of each glass specimen after irradiation with (a) 1 and (b) 10 Gy of X-rays.

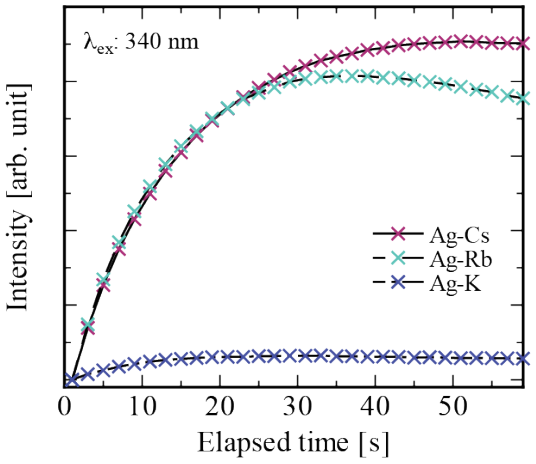


Fig. 6. (Color online) Change in RPL emission intensity with elapsed time. The excitation and monitoring wavelengths were 340 ± 20 nm and 400–900 nm, respectively.

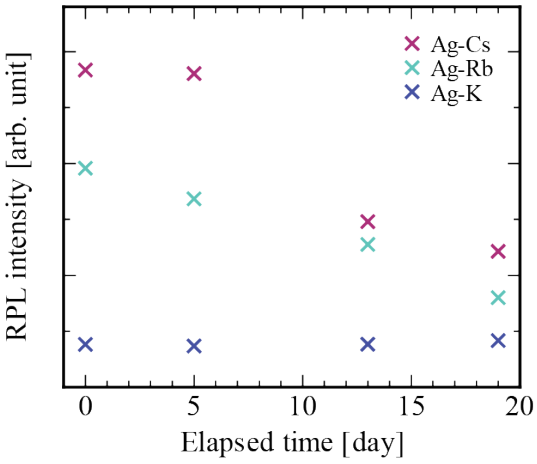


Fig. 7. (Color online) Fading characteristics of RPL emission at 620 nm for each glass specimen. The excitation wavelength was 340 ± 20 nm, and the monitored emission was the $Ag^{2+}$ emission at around 620 nm.

other words, it would be ideal if the build-up phenomenon does not occur. Therefore, the fast build-up of this specimen is a noteworthy feature.

Figure 7 shows the variation in luminescence intensity as a function of the elapsed time after 10 Gy of X-ray irradiation for each glass specimen. The excitation wavelength was 340 ± 20 nm, and the monitored emission was the $Ag^{2+}$ emission at around 620 nm for each glass specimen. No fading was observed for the Ag–K specimen in the present measurement period. On the other hand, the RPL intensities of the Ag–Rb and Ag–Cs specimens decreased to approximately half of the initial value after 20 days. In general, commercially available FD-7 is known to show minimal fading, and its fading has been reported to be less than 5% per year.[28] Therefore, the fading of the glass specimens in this study is faster than that of FD-7. However, the commercially available OSL imaging material, Eu:BaFBr (Fujifilm), fades at around 60% per day. On the other hand, even the Ag–Cs specimen, which shows the strongest fading among our glass specimens, attenuates only approximately 25% in one week. Therefore, it can be considered that the fading characteristics of the glass specimens are sufficient for X-ray imaging applications that do not necessitate the long-term measurement of radiation exposure.[41,42]

Figure 8 shows the TSL glow curves of all glass specimens. Among all the glass specimens, the glow peak area of Ag–K was the largest, and the obtained glow peaks tended to decrease as the $Z_{eff}$ of the specimen increased. On the other hand, FD-7 showed almost no luminescence. TSL is a phenomenon in which electrons and holes that are accumulated in the trapping centers by irradiation are re-excited by heat and emit photons. In other words, this result suggests that the Ag–K, Ag–Rb, and Ag–Cs specimens may contain a higher number of trapping centers than FD-7. In Table 2, although the $Z_{eff}^4$ of the Ag–Cs specimen was much higher than that of FD-7, there was no significant difference in $\Delta A_{abs}$, and the $\Delta A_{abs}$ values of the Ag–Rb and Ag–K specimens were very much equal to that of FD-7. This is because some of the electron–hole pairs

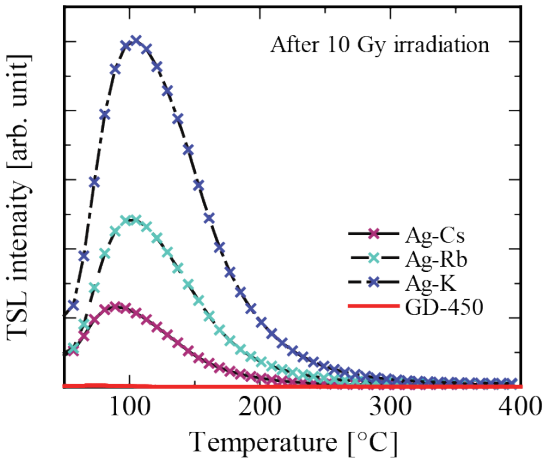


Fig. 8. (Color online) TSL glow curves of all glass specimens after X-ray irradiation.

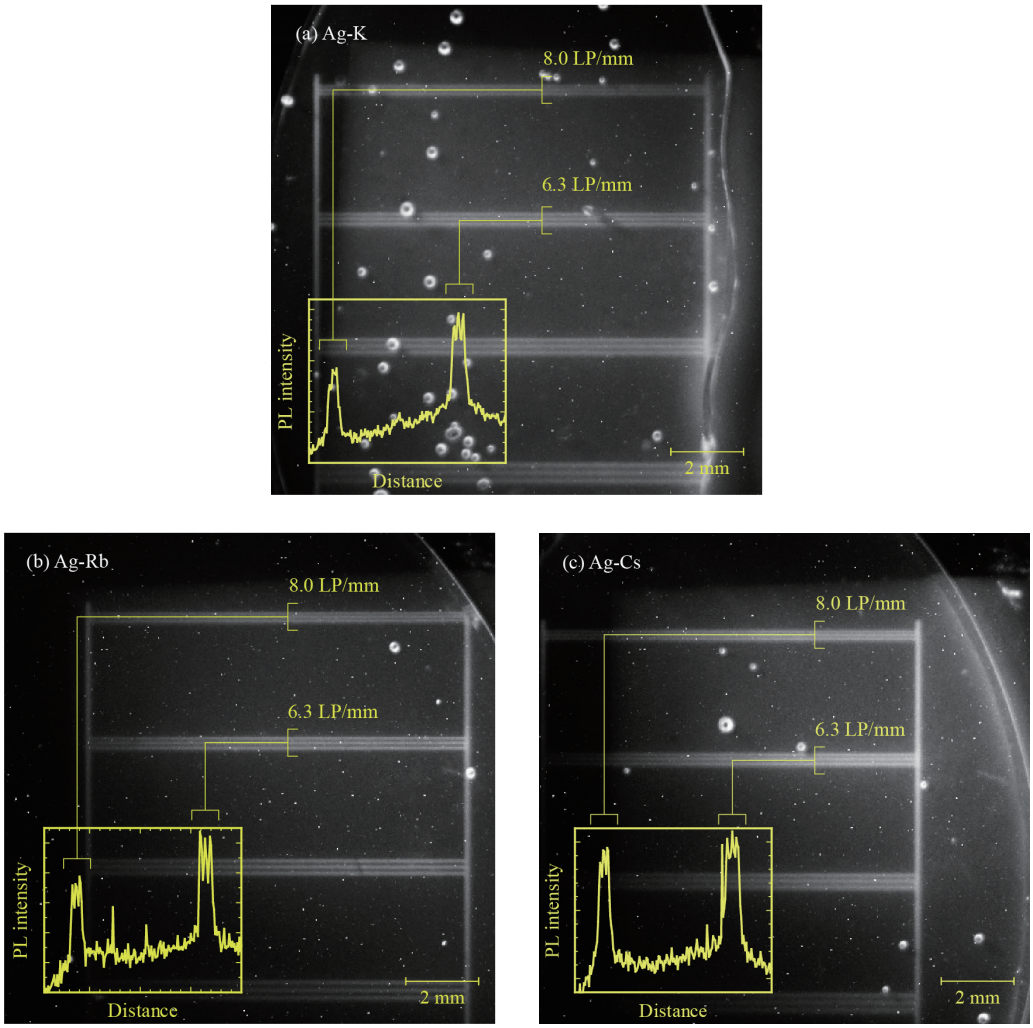


Fig. 9. (Color online) Resolution test of the X-ray images of the (a) Ag–K, (b) Ag–Rb, and (c) Ag–Cs specimens using the X-ray test chart. The inset shows the luminance on an arbitrary line perpendicular to the test line on the image.

induced by X-ray irradiation were trapped in trapping centers not associated with Ag and did not contribute to the formation of $Ag^{2+}$, resulting in a lower efficiency of $Ag^{2+}$ formation for the Ag–K, Ag–Rb, and Ag–Cs specimens than for FD-7.

Figure 9 shows the results of the resolution test for X-ray images. Resolution (LP/mm) is defined as the reciprocal of the width of the line pairs that can be found to be resolved in the image. The four-line pairs in the figure are 4.0, 5.0, 6.3, and 8.0 LP/mm from the bottom, and here, we focus on the line patterns of 6.3 and 8.0 LP/mm. From the histogram of the luminance on the line perpendicular to each line pattern, we concluded that the spatial resolutions of the specimens were 6.3 LP/mm for Ag–K and 8.0 LP/mm for both Ag–Rb and Ag–Cs. These resolutions are comparable to those of commercially available imaging plates, and an image with a higher resolution can be obtained by reading with a laser or other devices. The white dots seen in the image are voids in the glass, and the number of voids seems to be larger for the specimens with lighter alkali metal species. On the basis of the $T_g$ of the specimens, it is assumed that this is because Ag–K, which has a higher $T_g$, is more difficult to refine than Ag–Rb and Ag–Cs owing to the higher viscosity of the melt.

## 4. Conclusions

In this study, we succeeded in developing heavy-element-based RPL glass for X-ray imaging applications. RPL was observed in all the glass specimens, among which the Ag–Cs specimen showed the most prominent RPL emission. The resolution test in X-ray imaging revealed that the Ag–Rb and Ag–Cs specimens have a spatial resolution of at least 8 LP/mm. Although this imaging was conducted with a simple setup, we believe that images with a higher resolution can be obtained with an optical microscope. Furthermore, the fading of the omission from RPL centers was much lesser than that of commercial imaging plates, and the build-up took around 60 s to complete. We will try to reduce the fading and build-up through further detailed compositional studies.

## Acknowledgments

This work was supported by Grants-in-Aid for Scientific Research B (19H03533, 21H03733, and 21H03736), Early-Career Scientists (20K20104), and JSPS Fellows (20J23225). The Cooperative Research Project of the Research Center for Biomedical Engineering is also acknowledged.

## References

1 S. Basu, T. C. Kwee, S. Surti, E. A. Akin, D. Yoo, and A. Alavi: Ann. N. Y. Acad. Sci. **1228** (2011) 1. https://doi.org/10.1111/j.1749-6632.2011.06077.x

2 P. Moskal, N. Zoń, T. Bednarski, P. Białas, E. Czerwiński, A. Gajos, D. Kamińska, Ł. Kapłon, A. Kochanowski, G. Korcyl, J. Kowal, P. Kowalski, T. Kozik, W. Krzemień, E. Kubicz, S. Niedźwiecki, M. Pałka, L. Raczyński, Z. Rudy, O. Rundel, P. Salabura, N. G. Sharma, M. Silarski, A. Słomski, J. Smyrski, A. Strzelecki, A. Wieczorek, W. Wiślicki, and M. Zieliński: Nucl. Instrum. Method Phys. Res., Sect. A **775** (2015) 54. https://doi.org/10.1016/j.nima.2014.12.005

3 P. Lecoq: Nucl. Instrum. Method Phys. Res., Sect. A **809** (2016) 130. https://doi.org/10.1016/j.nima.2015.08.041

4 D. R. Schaart, H. T. van Dam, S. Seifert, R. Vinke, P. Dendooven, H. Löhner, and F. J. Beekman: Phys. Med. Biol. **54** (2009) 3501. https://doi.org/10.1088/0031-9155/54/11/015
5 A. Khan, P. Q. Vuong, G. Rooh, H. J. Kim, and S. Kim: J. Alloys Compd. **827** (2020) 154366. https://doi.org/10.1016/j.jallcom.2020.154366
6 K. Nomura, T. Ikegami, and N. Juto: Radioisotopes **51** (2002) 85.
7 H. Yasuda, K. Yajima, and T. Sato: Radiat. Meas. **134** (2020) 106309. https://doi.org/10.1016/j.radmeas.2020.106309
8 C. L. Silva-Fierro, D. Cortés-Elvira, E. López-Pineda, and M. E. Brandan: Proc. XVI Mex. Symp. Med. Phys. (AIP Conference Proceedings, 2021), p. 050025.
9 I. Ogawa, R. Hazama, H. Miyawaki, S. Shiomi, N. Suzuki, Y. Ishikawa, G. Kunitomi, Y. Tanaka, M. Itamura, K. Matsuoka, S. Ajimura, T. Kishimoto, H. Ejiri, N. Kudomi, K. Kume, H. Ohsumi, and K. Fushimi: Nucl. Phys. A **730** (2004) 215. https://doi.org/10.1016/j.nuclphysa.2003.10.015
10 N. J. C. Spooner, G. J. Davies, J. D. Davies, G. J. Pyle, T. D. Bucknell, G. T. A. Squier, J. D. Lewin, and P. F. Smith: Phys. Lett. B **321** (1994) 156. https://doi.org/10.1016/0370-2693(94)90343-3
11 F. Ariztizabal, M. Bosman, M. Cavalli-Sforza, I. Efthymiopoulos, C. Padilla, F. Teubert, R. Arsenescu, C. Blag, V. Boldea, S. Dita, Z. Ajaltouni, F. Badaud, N. Bouhemaid, P. Brette, M. Brossard, R. Chadelas, J. C. Chevaleyre, M. Crouau, F. Daudon, J. J. Dugne, B. Michel, G. Montarou, G. S. Muanza, D. Pallin, S. Poirot, L. P. Says, F. Vazeille, O. Gildemeister, A. Henriques, J. Ivarsson, M. Nessi, L. Poggioli, P. Sonderegger, A. Amorim, P. Ferreira, A. Gomes, A. Maio, L. Peralta, M. David, M. Kostrikov, M. Kulagin, V. Lapin, Y. Protopopov, A. Solodkov, A. Zaitsev, R. Leitner, M. Suk, P. Tas, L. Caloba, M. Gaspar, F. Marroquin, A. Pereira, J. M. Seixas, Z. Thome, and H. Hakopian: Nucl. Instrum. Method Phys. Res., Sect. A **349** (1994) 384. https://doi.org/10.1016/0168-9002(94)91201-7
12 V. D. Ryzhikov, A. D. Opolonin, P. V. Pashko, V. M. Svishch, V. G. Volkov, E. K. Lysetskaya, D. N. Kozin, and C. Smith: Nucl. Instrum. Method Phys. Res., Sect. A **537** (2005) 424. https://doi.org/10.1016/j.nima.2004.08.056
13 L. E. Sinclair, D. S. Hanna, A. M. L. MacLeod, and P. R. B. Saull: IEEE Trans. Nucl. Sci. **56** (2009) 1262. https://doi.org/10.1109/TNS.2009.2019271
14 T. Yanagida, Y. Fujimoto, S. Kurosawa, K. Kamada, H. Takahashi, Y. Fukazawa, M. Nikl, and V. Chani: Jpn. J. Appl. Phys. **52** (2013) 076401. https://doi.org/10.7567/JJAP.52.076401
15 C. L. Melcher, J. S. Schweitzer, R. S. Manente, and C. A. Peterson: IEEE Trans. Nucl. Sci. **38** (1991) 506. https://doi.org/10.1109/23.289349
16 T. Anniyev, M. Vasilyev, V. Khabashesku, and F. Inanc: IEEE Trans. Nucl. Sci. **67** (2020) 1885. https://doi.org/10.1109/TNS.2020.3007125
17 T. Yanagida, T. Kato, Y. Takebuchi, D. Nakauchi, and N. Kawaguchi: Radiat. Meas. **132** (2020) 106250. https://doi.org/10.1016/j.radmeas.2020.106250
18 H. Kimura, F. Nakamura, T. Kato, D. Nakauchi, G. Okada, N. Kawaguchi, and T. Yanagida: Sens. Mater. **30** (2018) 1555. https://doi.org/10.18494/SAM.2018.1923
19 D. Shiratori, Y. Isokawa, H. Samizo, G. Okada, N. Kawaguchi, and T. Yanagida: J. Mater. Sci.: Mater. Electron. **30** (2019) 2464. https://doi.org/10.1007/s10854-018-0520-0
20 A. Vedda, N. Chiodini, D. Di Martino, M. Fasoli, L. Griguta, F. Moretti, and E. Rosetta: J. Non. Cryst. Solids **351** (2005) 3699. https://doi.org/10.1016/j.jnoncrysol.2005.10.001
21 D. Shiratori, T. Kato, D. Nakauchi, N. Kawaguchi, and T. Yanagida: Sens. Mater. **33** (2021) 2171. https://doi.org/10.18494/SAM.2021.3317
22 Y. Takebuchi, H. Fukushima, T. Kato, D. Nakauchi, N. Kawaguchi, and T. Yanagida: Sens. Mater. **32** (2020) 1405. https://doi.org/10.18494/SAM.2020.2717
23 G. Okada, K. Hirasawa, T. Yanagida, and H. Nanto: Sens. Mater. **33** (2021) 2117. https://doi.org/10.18494/SAM.2021.3327
24 C. C. Gronchi, S. G. P. Cecatti, T. C. N. O. Pinto, and L. V. E. Caldas: Nucl. Instrum. Method Phys. Res., Sect. B **266** (2008) 2915. https://doi.org/10.1016/j.nimb.2008.03.139
25 H. Kimura, T. Kato, D. Nakauchi, N. Kawaguchi, and T. Yanagida: Sens. Mater. **33** (2021) 2187. https://doi.org/10.18494/SAM.2021.3322
26 Y. Miyamoto, T. Ohno, Y. Takei, H. Nanto, T. Kurobori, T. Yanagida, A. Yoshikawa, Y. Nagashima, and T. Yamamoto: Radiat. Meas. **55** (2013) 72. https://doi.org/10.1016/j.radmeas.2012.10.018
27 T. Kurobori, W. Zheng, Y. Miyamoto, H. Nanto, and T. Yamamoto: Opt. Mater. **32** (2010) 1231. https://doi.org/10.1016/j.optmat.2010.04.004
28 D. Y. C. Huang and S. M. Hsu: Adv. Cancer Ther. (InTech, 2011).
29 K. Takahashi, A. Osaka, and S. Hayashi: J. Ceram. Assoc. Jpn. **90** (1982) 51. https://doi.org/10.2109/jcersj1950.90.1038_51

30 N. Soga, K. Tanaka, and R. Ota: J. Soc. Mater. Sci. Jpn. **35** (1986) 133. https://doi.org/10.2472/jsms.35.133
31 N. Kitamura, T. Sakamoto, and H. Takebe: Mater. Trans. **59** (2018) 437. https://doi.org/10.2320/matertrans.M-M2017854
32 E. Mura, J. Lousteau, D. Milanese, S. Abrate, and V. M. Sglavo: J. Non. Cryst. Solids **362** (2013) 147. https://doi.org/10.1016/J.JNONCRYSOL.2012.11.029
33 M. Lu, F. Wang, K. Chen, Y. Dai, Q. Liao, and H. Zhu: Spectrochim. Acta Part A Mol. Biomol. Spectrosc. **148** (2015) 1. https://doi.org/10.1016/J.SAA.2015.03.121
34 W. Zheng and T. Kurobori: J. Lumin. **131** (2011) 36. https://doi.org/10.1016/j.jlumin.2010.08.024
35 W. Zheng and T. Kurobori: Nucl. Instrum. Method Phys. Res., Sect. B **269** (2011) 2814. https://doi.org/10.1016/j.nimb.2011.08.019
36 Y. Miyamoto, T. Yamamoto, K. Kinoshita, S. Koyama, Y. Takei, H. Nanto, Y. Shimotsuma, M. Sakakura, K. Miura, and K. Hirao: Radiat. Meas. **45** (2010) 546. https://doi.org/10.1016/j.radmeas.2010.01.012
37 D. Shiratori, Y. Isokawa, H. Samizo, N. Kawaguchi, and T. Yanagida: J. Ceram. Soc. Jpn. **127** (2019) 455. https://doi.org/10.2109/jcersj2.19058
38 H. Tatsumi, G. Okada, T. Yanagida, and H. Masai: Chem. Lett. **45** (2016) 280. https://doi.org/10.1246/cl.151078
39 H. Kawamoto, Y. Fujimoto, M. Koshimizu, G. Okada, T. Yanagida, and K. Asai: Jpn. J. Appl. Phys. **58** (2019) 062003. https://doi.org/10.7567/1347-4065/ab0c84
40 T. Kato, D. Shiratori, M. Iwao, H. Takase, D. Nakauchi, N. Kawaguchi, and T. Yanagida: Sens. Mater. **33** (2021) 2163. https://doi.org/10.18494/SAM.2021.3318
41 H. Ohuchi: Jpn. J. Heal. Phys. **34** (1999) 52. https://doi.org/10.5453/jhps.34.52
42 M. Kishimoto, T. Nakamura, K. Toh, K. Sakasai, M. Katagiri, H. Takahashi, and M. Nakazawa: J. At. Energy Soc. Jpn. **43** (2001) 168. https://doi.org/10.3327/jaesj.43.168